

# Near-IR and Visual High Resolution Polarimetric Imaging with AO Systems

Hans M. Schmid

Institute for Particle Physics and Astrophysics, ETH Zurich,  
Wolfgang-Pauli-Str. 27, 8093 Zurich, Switzerland

**Abstract.** Many spectacular polarimetric images have been obtained in recent years with adaptive optics (AO) instruments at large telescopes because they profit significantly from the high spatial resolution. This paper summarizes some basic principles for AO polarimetry, discusses challenges and limitations of these systems, and describes results which illustrate the performance of AO polarimeters for the investigation of circumstellar disks, of dusty winds from evolved stars, and for the search of reflecting extra-solar planets.

**Keywords.** polarimetry, AO systems, high resolution, high contrast, scattering, circumstellar disks, stellar winds, reflecting planets

---

## 1. Science drivers for AO polarimetry

Pushing observations to higher spatial resolution is a key for progress for the investigation of the geometry and the physics of extended objects in astronomy. The diffraction limited angular resolution of a telescope is given by the ratio between wavelength and the telescope diameter  $\mathcal{R} \approx \lambda/D$ . High resolution  $\mathcal{R} \lesssim 0.1''$  imaging polarimetry in the visual to near-IR range requires therefore large telescopes on the ground equipped with adaptive optics (AO) systems for the correction of the atmospheric seeing or observations at  $\lambda < 1 \mu\text{m}$  with the Hubble Space Telescope (HST). This review focuses on the recent, significant technical progress achieved with imaging polarimeters using AO systems at large ground based telescopes.

The goal of AO systems is the correction of the wavefront deformations introduced by the atmospheric turbulence with a control loop (Fig. 1), which measures the deviations with a wavefront sensor (WFS), calculates the corrections with a real time computer (RTC), and applies them to a deformable mirror (DM). This correction must be faster than the turbulence time scale of a few milli-seconds and this requires a bright photon source close to the science target. The central stars of a circumstellar disk or shell, or a planetary system are ideal wave front probes for good AO observations.

The AO system converts the seeing disk of a star into a point spread function (PSF) with a diffraction limited core with a width of  $\approx \mathcal{R}$  and a residual halo with about the size of the initial seeing disk (e.g. Davies & Kasper 2012). For an 8 m telescope  $\mathcal{R}$  is  $\approx 17$  mas in the R-band ( $\lambda = 0.65 \mu\text{m}$ ) and  $\approx 42$  mas in the H-band ( $1.6 \mu\text{m}$ ).

The performance of an AO system is described by the Strehl ratio  $S$ , which is roughly the fraction of light concentrated in the PSF core.  $S$  depends for a given system strongly on  $\lambda$ , for example VLT-SPHERE reaches for a bright guide star under excellent atmospheric conditions up to  $S \approx 0.9$  in the H-band but only  $S \approx 0.6$  for the R-band (Fusco et al. 2016) and therefore the PSF halo is stronger at shorter wavelengths. The AO performance depends also on the seeing and already average conditions can reduce  $S$  by 30–50 %. The Strehl ratio is also reduced for faint guide stars (e.g.  $> 12^m$ ) because of the lack of photons for accurate wave front measurements (Milli et al. 2017).

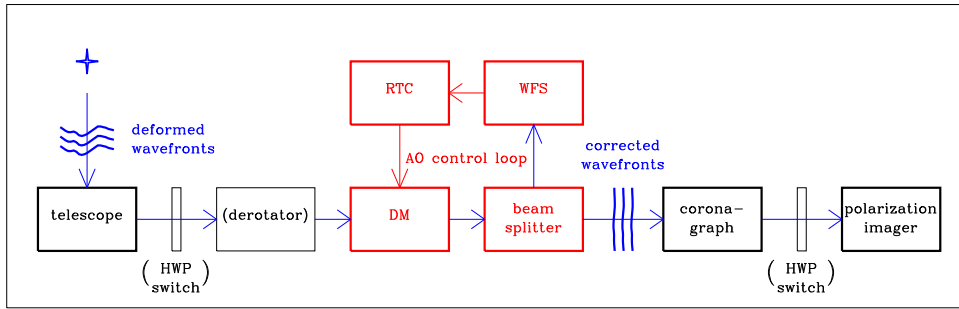


**Figure 1.** Light path and schematic block diagram for a telescope with AO system, coronagraph, and polarimetric imager. Possible locations of a half wave plate (HWP) switch and a derotator are indicated (DM: deformable mirror, WFS: wave front sensor, RTC: real time computer).

The PSF core is typically so bright, that sensitive observations of the stellar surroundings would heavily saturate the detector. Many observations require therefore a stellar coronagraph (Fig. 1) to block the light of the PSF core for  $r \lesssim 0.1''$ . For extreme AO systems, like Gemini-GPI and VLT-SPHERE, the coronagraphs suppress also the diffraction pattern of the PSF at separations  $r \approx 0.1''$  to  $0.4''$  (Sivaramakrishnan et al. 2001).

The residual PSF halo is variable and typically stronger than the signal of a faint companion, a disk, or the dusty stellar wind. Differential techniques are required to disentangle the light of a target from the halo of the central star (e.g. Racine et al. 1999) and polarimetry is an ideal differential technique to distinguish between the polarized scattered light of a faint circumstellar target and the direct (and usually unpolarized) light of the bright central star.

The main science drivers for AO polarimetry are:

- Bright stars with circumstellar scattering are ideal for a very good AO performance and often very interesting targets for polarimetric investigations.
- Separating and resolving circumstellar scattering regions from the star enhances significantly the measurable polarization signal.
- Polarimetry is an ideal differential technique for high contrast observations of polarized sources.
- Often it is much easier to detect and image a target with differential polarimetry, while measurements of the intensity requires a follow-up in a second step.

## 2. Technical challenges for polarimetry with AO systems

### 2.1. Historical developments

The first AO systems with polarimetric modes were the Cassegrain instrument Subaru-CIAO (Murakawa et al. 2004) and the Nasmyth instrument VLT-NACO (Lenzen et al. 2003), and they delivered very promising polarimetric result for disks and circumstellar shells (Apai et al. 2004, Murakawa et al. 2005). They also showed that simultaneous measurements of opposite polarization modes  $I_{\perp}$  and  $I_{\parallel}$ , and the polarimetric self-calibration with a half wave plate (HWP) switch are essential for good results, and that the calibration of systematic polarization effects for the Nasmyth instrument NACO is difficult (Witzel et al. 2011). This triggered efforts for better correction procedures for the polarization of the Nasmyth instruments VLT-NACO and Subaru-HiCIAO and disk images with much higher quality were achieved (e.g. Quanz et al. 2011, Hashimoto et al. 2011, Muto et al. 2012). In addition, the lessons learned from the “early” AO po-

**Table 1.** Rough parameters for widely used AO polarimeters, which are available or were available until recently at 8m class telescopes.

	Subaru	Gemini-South	VLT-SPHERE <sup>1</sup>	
	HiCIAO <sup>2</sup>	GPI <sup>3</sup>	IRDIS <sup>4</sup>	ZIMPOL <sup>5</sup>
AO system	AO188 <sup>6</sup>	(GPI)	SAXO <sup>7</sup>	
in operation	2009-2015	2013-2020 <sup>a</sup>	since 2015	
DM actuators	188	43 × 43	41 × 41	
Strehl ratio <sup>b</sup>	≈ 0.4, H-band <sup>6</sup>	≈ 0.9, H-band <sup>3</sup>	≈ 0.9, H-band <sup>7,8</sup>	≈ 0.6, R-band <sup>7,8</sup>
guide star limit <sup>c</sup>	$I < 11^{\text{mag}}$	$I < 10^{\text{mag}}$	$R < 14^{\text{mag}}$	$R < 11^{\text{mag}}$
coronagraphy	X	X	X	X
polarimetric imager				
polarimetry type	double beam	integral field pol. <sup>9</sup>	double beam <sup>4</sup>	fast modulation <sup>5</sup>
wavelength range	0.85 – 2.5 $\mu\text{m}$	0.9 – 2.3 $\mu\text{m}$	1.0 – 2.3 $\mu\text{m}$	0.52 – 0.9 $\mu\text{m}$
spatial resolution	40 – 60 mas	30 – 60 mas	30 – 60 mas	20 – 25 mas
field of view	10'' × 20''	2.7'' × 2.7''	11'' × 11''	3.6'' × 3.6''
telescope and instrument polarization				
focal station	Nasmyth	Cassegrain	Nasmyth	
HWP switch	after AO	after AO	before derotator and AO	
telescope polarization	moderate	small <sup>10</sup>	moderate <sup>11</sup>	large/compensated <sup>5,12</sup>
derotator cross talks	large	none	large <sup>12</sup>	large/controlled <sup>12</sup>

Notes: <sup>a</sup>at Gemini-South, will be upgraded and mounted at Gemini-North in future, <sup>b</sup>for a bright guide star and excellent atmospheric conditions, <sup>c</sup>Strehl ratio degraded by a factor of  $\approx 2$  because of guide star “faintness”  
References: <sup>1</sup>Beuzit et al. 2019, <sup>2</sup>Hodapp et al. 2008, <sup>3</sup>Macintosh et al. 2014, <sup>4</sup>Dohlen et al. 2008, <sup>5</sup>Schmid et al. 2018, <sup>6</sup>Suzuki et al. 2010, <sup>7</sup>Fusco et al. 2016, <sup>8</sup>Milli et al. 2017, <sup>9</sup>Perrin et al. 2015, <sup>10</sup>Wiktorowicz et al. 2014, <sup>11</sup>de Boer et al. 2020, <sup>12</sup>Bazzon et al. 2012.

larimeters were considered for the designs of the subsequent extreme AO instruments Gemini-GPI (Macintosh et al. 2014) and VLT-SPHERE (Beuzit et al. 2019) which provide currently the best performance in AO polarimetry.

Table 1 lists key system parameters and corresponding references of widely used systems, which produced a large fraction of the recent scientific result in AO polarimetry. The table illustrates the progress in AO performance from the older Subaru-HiCIAO system (the parameters of VLT-NACO are similar), to the newer extreme AO systems Gemini-GPI and VLT-SPHERE. Also of interest are the very different polarimetric designs of the instruments, which are described below.

## 2.2. Polarization imagers

*Double beam polarimeters* for linear polarization measurements are based on a polarization beam splitter, often a Wollaston prism, and a rotating HWP. This provides two images side by side on the detector with “opposite” polarization intensities  $I_{\perp}$  and  $I_{\parallel}$  from which one can determine the differential signal  $I_{\perp} - I_{\parallel}$ . The two images are taken simultaneously and this is essential for the suppression of the strongly variable speckle noise present in AO observations. The HWP is used for the selection of the Stokes  $Q=I_0 - I_{90}$  and  $U=I_{45} - I_{135}$  parameters and as switch for the compensation of the instrument polarization  $q_{\text{inst}}I$  and  $u_{\text{inst}}I$ . A rotation of the HWP by  $45^\circ$  switches the sign of the incoming  $Q_{\text{in}}$ -signal (or  $U_{\text{in}}$ ) for two consecutive measurements  $Q^+$  and  $Q^-$ , while the instrument polarization remains unchanged. The difference

$$Q^+ - Q^- = (Q_{\text{in}} + q_{\text{inst}}I) - (-Q_{\text{in}} + q_{\text{inst}}I) = 2Q_{\text{in}}$$

compensates then the instrumental polarization. The use of a HWP switch is essential for all AO polarimeters. The basic double beam set-up was used by the “early” AO polarimeters Subaru-CIAO and VLT-NACO, but also for Subaru-HiCIAO. For SPHERE-IRDIS the principle is the same, but it uses a “grey” beam splitter plate and polarizers to avoid the differential aberrations of a Wollaston prism between the two beams (Dohlen et al. 2008). Double beam polarimeters provide a high efficiency and typically a large field of view.

*Integral field polarimeter:* This is an innovative concept used as polarimetric mode in combination with the integral field spectrograph (IFS) of Gemini-GPI which proved to work very successfully (Perrin et al. 2015). The IFS uses a 2D-array of micro-lenses in the focal plane, producing spots which are then dispersed with a grism producing an array of about 36 000 low resolution spectra on the detector. In polarimetric mode, the grism is replaced by a Wollaston prism producing an array of double spots with “opposite” polarizations  $I_{\perp}$  and  $I_{\parallel}$  instead of the low resolution spectra. The field of view is given by the focal plane sampling of the micro-lens array which is smaller (for a given detector size) than for the “standard” double beam polarimeters.

*Fast modulation polarimeter:* SPHERE-ZIMPOL is based on a fast polarization modulation concept using a liquid crystal device and a polarizer, which converts the polarization modulation into an intensity modulation between  $I_{\perp}$  and  $I_{\parallel}$ . A CCD-detector is used for the signal demodulation with the main advantage that  $I_{\perp}$  and  $I_{\parallel}$  are registered with the same detector pixels so that flat-fielding effects are minimized. The modulation is faster than the speckle variations and  $I_{\perp}$  and  $I_{\parallel}$  are registered essentially simultaneously (Schmid et al. 2018). The system is optimized in various ways for polarimetry, achieves a high dynamic range and a very high sensitivity of  $10^{-5}$  for the search of reflecting planets around bright nearby stars in the visual range. Less good, when compared to double beam imagers, are the parameters for the polarimetric efficiency (70–90 %), the small field of view, and the bright guide star limit for the AO system, because ZIMPOL shares the light with the visual WFS.

### 2.3. Telescope and instrument polarization effects

“Smart” polarimeters have a simple design which minimizes telescope and instrument polarization effects with a Cassegrain instrument and a straight through beam. Subaru-CIAO (Murakawa et al. 2004) and Gemini-GPI (Perrin et al. 2015) followed as far as possible this principle and therefore the polarimetric calibration of the data is relatively simple (e.g. Wiktorowicz et al. 2014).

All other systems in Table 1 are “not smart”, but complex, large, and located at the Nasmyth focus because this is favorable for many AO aspects. Therefore, the telescope and instrument polarization effects are complicated and require a good concept for the measurements of the polarization without compromising the performance of the AO system and the coronagraph. A few typical problems are:

- the polarization effects of the inclined telescope mirror M3 for Nasmyth systems,
- “rotating” instrument polarization effects introduced by an image derotator,
- static instrument polarization effects from inclined optical components.

There are many ways how these problems can be solved and each system must be considered individually. The HWP switch discussed for the polarization imagers can be placed early in the beam (Fig. 1) to compensate for the instrument polarization of many components. However, this approach does not correct for polarization cross-talks, in particular the substantial conversion from linear to circular polarization by the inclined mirrors of an image derotator. Therefore, a derotator can strongly reduce the measurable linear polarization depending on its orientation (de Boer et al. 2020), which must be corrected with detailed hardware calibrations. Also the Nasmyth telescope mirror M3 requires polarimetric corrections (e.g. Joos et al. 2008), which must be derived or at least verified with standard star data. Extremely helpful for the polarimetric calibration of many data sets are objects with an unpolarized central star which serves as zero polarization reference source.

For SPHERE-IRDIS there are moderate telescope and strong derotator polarization effects which can be corrected with a data reduction package based on a detailed polar-

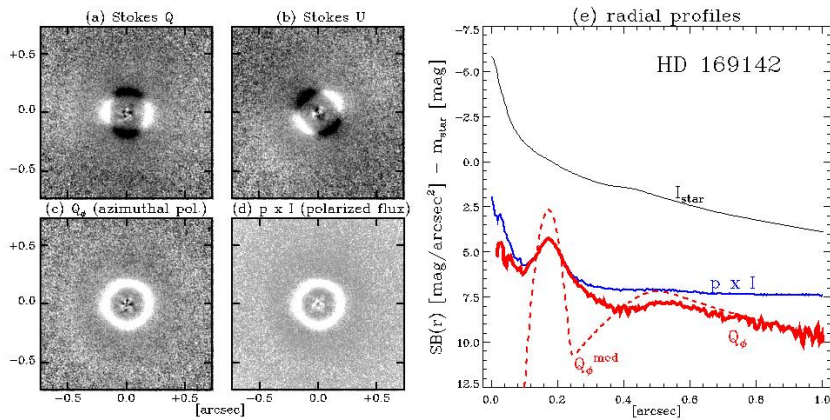


**Figure 2.** Images for (a)  $Q$ , (b)  $U$ , (c)  $Q_\phi$ , and (d)  $p \times I$  for the pole-on disk HD 169142 with a bright inner disk wall at  $r = 0.17''$  and an outer low surface brightness disk. Panel (e) gives azimuthally averaged radial profiles for  $Q_\phi$ ,  $p \times I$ , the stellar PSF  $I_{\text{star}}$ , and a model for the intrinsic  $Q_\phi^{\text{mod}}$  (Tschudi & Schmid 2021), which fits after convolution the observed  $Q_\phi$  curve.

ization model of the whole instrument (van Holstein et al. 2020). SPHERE-ZIMPOL uses three additional HWPs and one polarization compensator plate, which actively correct for the strong telescope polarization and derotator effects (Bazzon et al. 2012).

#### 2.4. Quantitative polarimetric measurements

Often only differential polarization images  $Q_{\text{cs}}(\alpha, \delta)$  and  $U_{\text{cs}}(\alpha, \delta)$  of a circumstellar scattering source are available because the intensity  $I_{\text{cs}}$  cannot be disentangled from the bright and highly variable PSF of the central star. The quantitative analysis of  $Q_{\text{cs}}$  and  $U_{\text{cs}}$  must take noise bias effects and the polarimetric cancellation into account.

If the  $Q_{\text{cs}}$  and  $U_{\text{cs}}$  images are noisy then the determination of the polarized flux according to  $p_{\text{cs}} \times I_{\text{cs}} = (Q_{\text{cs}}^2 + U_{\text{cs}}^2)^{1/2}$  is strongly biased upward (Simmons & Stewart 1985) as can be seen in Fig. 2 for the outer disk. This problem can be avoided with the use of the azimuthal polarization parameters  $Q_\phi, U_\phi$ . For circumstellar scattering the polarization is essentially in azimuthal direction described by  $Q_\phi$  and the  $U_\phi$ -signal is very small. Therefore, the  $Q_\phi$ -signal is a very good approximation of the polarized flux  $Q_\phi \approx p_{\text{cs}} \times I_{\text{cs}}$  and this parameter avoids the noise bias (Schmid et al. 2006a).

The measurable polarization  $Q_{\text{cs}}, U_{\text{cs}}$  is also affected by the limited observational resolution, which introduces smearing and for polarimetry also a cancellation between image regions with  $+Q$  and  $-Q$  or  $+U$  and  $-U$  signals (Schmid et al. 2006a). This effect can be very substantial for AO polarimetry of compact sources as shown in Fig. 2(e) for the inner ring of HD 169142. There, the measurable signal  $Q_\phi$  is about 4 times smaller than the model for the intrinsic signal  $Q_\phi^{\text{mod}}$  before convolution with the PSF. For the more extended disk the cancellation effect is much reduced. This effect depends strongly on the atmospheric conditions, but can be modeled and corrected well, if the PSF is known accurately (Tschudi & Schmid 2021).

### 3. Scientific results

#### 3.1. Protoplanetary disks

Protoplanetary disk are the “easy targets” for polarimetric imaging with AO systems especially the so-called transition disks. They have a large central cavity and the strongly

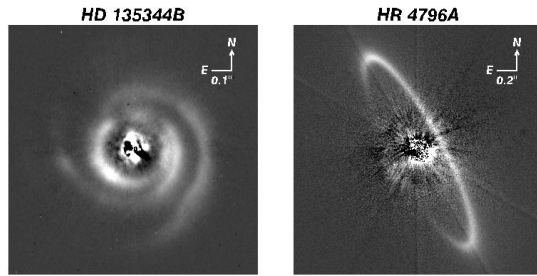


**Figure 3.**  $Q_\phi$ -images of (a) the protoplanetary spiral disk HD 135344B and (b) the bright debris disk HR 4796A. The data are described in Stolker et al. (2016) and Milli et al. (2019).

illuminated inner disk wall can be separated by  $d > 10$  AU from the star or  $> 0.1''$  for a disk in a nearby ( $d \approx 100$  pc) star forming region. The disk integrated polarized flux is up to  $Q_\phi/I_{\text{star}} \approx 1$  %.

The images show the scattering polarization of the dust in the surface layer of optically thick disks and they reveal a surprising diversity of hydrodynamical structures: central disk cavities (Quanz et al. 2011, Hashimoto et al. 2012), large scale spirals (Garufi et al. 2013, Benisty et al. 2015, Fig. 3), circular gaps (Quanz et al. 2013, Fig. 2), shadows from tilted disks near the star (Marino et al. 2015, Pinilla et al. 2018), and much more. Some structures are explained by the presence of newly formed planets and two young planets were indeed found in the large disk cavity of PDS 70 (Keppler et al. 2018). These images and corresponding ALMA maps are of much interest for the understanding of the planet formation processes in disks.

Well calibrated disk data provide the spectral dependence of the polarized reflectivity  $Q_{\text{disk}}(\lambda)/I_{\text{star}}(\lambda)$  and the few existing measurements indicate a “reddish” color (e.g. Hunziker et al. 2021). The fractional polarization  $p_{\text{disk}}$  of the reflected light was first measured with HST for AB Aur (Perrin et al. 2009) but this can now also be achieved with AO systems. Reported values for a scattering angle of  $\approx 90^\circ$  range from  $p_{\text{disk}} \approx 20 - 30$  % for visual wavelengths, to higher values  $p_{\text{disk}} \approx 30 - 60$  % in the near-IR (Monnier et al. 2019, Hunziker et al. 2021, Tschudi & Schmid 2021). More such quantitative measurements will become available and they will help to constrain the properties of the scattering dust.

### 3.2. Debris disks

Dust debris disk are signposts for the presence of colliding planetesimals around a star. Typically, we see the scattered light from dust rings at separations of  $\approx 10 - 100$  AU, sometimes surrounded by scattering halos from small grains blown out by radiation pressure. Debris disk are optically thin, with a low polarization contrast  $Q_\phi/I_\star \lesssim 0.05$  % (Engler et al. 2017) requiring deep observations with extreme AO systems like GPI or SPHERE. Edge-on systems are easier to detect because the large grains are strongly forward scattering (Esposito et al. 2020).

Debris disks with high inclination, like the bright system HR 4796A (Fig. 3), are ideal for the determination of the dust scattering phase function for the intensity and the polarization because the photons undergo only one scattering and the scattering angles are well defined (Perrin et al. 2015, Milli et al. 2019, Chen et al. 2020, Arriaga et al. 2020). Such data provide important information for model calculation of the light scattering by complex dust particles.

### 3.3. Dust formation in the stellar wind of red giants

Important processes for the mass loss from red giants are the formation of dust and the wind acceleration by the radiation pressure acting on dust grains. The light scattered by the dust can be directly observed with non-coronagraphic AO polarimetry. The key technical requirement is a high spatial resolution because the stellar diameters are only about 50 mas for the most extended red giants (e.g.  $\alpha$  Ori, Mira, W Hya, R Dor,  $\alpha$  Sco). This favors strongly observations at small  $\lambda$  with SPHERE-ZIMPOL (Tab. 1), which achieves a spatial resolution of ( $\mathcal{R} \approx 20$  mas). Interesting monitoring results are also obtained with an “AO free” system based on differential speckle polarimetry (Safonov et al. 2020) and very promising are the prospects for polarimetry using sparse aperture masking interferometry, which will achieve a spatial resolution of up to 10 mas with the new Subaru-SCeXAO-Vampires instrument (Norris et al. 2015).

The polarimetric observations show clumpy and variable dust structures, and the derived radial distribution defines the locations for dust formation and wind acceleration. From the color of the scattered light one can estimate the dust particle sizes (e.g. Ohnaka et al. 2016, Khouri et al. 2020).

### 3.4. Reflecting extrasolar planets

Light reflecting from planets is polarized and this offers the possibility for detecting extrasolar planets with high resolution polarimetry. The SPHERE-ZIMPOL instrument was optimized for this science case (Schmid et al. 2006b) and a search for extra-solar planets around the nearest bright stars  $\alpha$  Cen A and B, Sirius,  $\epsilon$  Eri, Altair and  $\tau$  Cet has been carried out by Hunziker et al. (2020). The requirements are extreme, for example a Jupiter-sized planet at a separation of 1 AU would produce only a polarimetric contrast of about  $C_{\text{pol}} = p_{\text{planet}} \times I_{\text{planet}} / I_{\text{star}} \approx 2 \cdot 10^{-8}$  (e.g. Buenzli & Schmid 2009). Such detection limit could be reached with an exposure time of  $t_{\text{exp}} = 3.4^h$  for  $\alpha$  Cen A but no successful detection has been achieved. However, it is shown that the ZIMPOL polarimetry is for  $r > 0.5''$  photon noise limited and the contrast limit should just improve with  $t_{\text{exp}}$  like  $C_{\text{limit}} \propto (t_{\text{exp}})^{-1/2}$ . Deeper searches for promising targets are therefore ongoing for  $\epsilon$  Eri b or the recently reported planet candidate around  $\alpha$  Cen A (Wagner et al. 2021).

## 4. Conclusions

High resolution polarimetric imaging with AO systems made in the last decade a major step forward from a special technique used by a few experts to a main stream observing mode offered by leading observatories to the astronomical community. Many astronomers use now this technique and they produced a continuous string of first class science results on circumstellar disks, dusty shells around evolved stars, and several other science topics not covered in this review.

AO polarimetry is not a simple observing technique, because of instrument polarization effects and the variable AO performance which depends on the atmospheric turbulence. In addition, many of the most interesting targets are very faint and very close to the bright central star. Despite these extreme challenges the results obtained with different systems agree very well, giving much credibility to this technique and proving its maturity.

This success will lead to more progress in the near and more distant future, like deeper observations for fainter targets, improved observing and calibration procedures for quantitative measurements, but also upgrades on existing instruments and hopefully the development of much more powerful AO polarimeters for the coming generation of extremely large telescopes.

## References

- Apai, D., Pascucci, I., Brandner, W., et al. 2004, *A&A*, 415, 671
- Arriaga, P., Fitzgerald, M. P., Duchêne, G., et al. 2020, *AJ*, 160, 79
- Bazzon, A., Gisler, D., Roelfsema, R., et al. 2012, *SPIE Proc.*, 8446, 844693
- Buenzli, E. & Schmid, H. M. 2009, *A&A*, 504, 259
- Benisty, M., Juhasz, A., Boccaletti, A., et al. 2015, *A&A*, 578, L6
- Beuzit, J.-L., Vigan, A., Mouillet, D., et al. 2019, *A&A*, 631, 155
- Chen, C., Mazoyer, J., Poteet, C. A., et al. 2020, *ApJ*, 898, 55
- Davies, R. & Kasper, M. 2012, *Ann.Rev.A&A*, 50, 305
- de Boer, J., Langlois, M., van Holstein, R. G., et al. 2020, *A&A*, 633
- Dohlen, K., Langlois, M., Saisse, M., et al. 2008, *SPIE Proc.*, 7014, 70143L
- Engler, N., Schmid, H. M., Thalmann, C., et al. 2017, *A&A*, 607, 90
- Esposito, T. M., Kalas, P., Fitzgerald, M. P., et al. 2020, *AJ*, 160, 24
- Fusco, T., Sauvage, J.-F., Mouillet, D., et al. 2016, *SPIE Proc.*, 9909, 99090U
- Garufi, A., Quanz, S. P., Avenhaus, H., et al. 2013, *A&A*, 560, 105
- Hashimoto, J., Tamura, M., Muto, T., et al. 2011, *ApJ (Letters)*, 729, L17
- Hashimoto, J., Dong, R., Kudo, T., et al. 2012, *ApJ (Letters)*, 758, L19
- Hodapp, K. W., Suzuki, R., Tamura, M., et al. 2008, *SPIE Proc.*, 7014, 701419
- Hunziker, S., Schmid, H. M., Mouillet, D., et al. 2020, *A&A*, 634, 69
- Hunziker, S., Schmid, H. M., Ma, J., et al. 2021, *A&A*, 648, 110
- Joos, F., Buenzli, E., Schmid, H. M., et al. 2008, *SPIE Proc.*, 7016, 70161I
- Keppler, M., Benisty, M., Müller, A., et al. 2018, *A&A*, 617, A44
- Khoury, T., Vlemmings, W. H. T., Paladini, C., et al. 2020, *A&A*, 635, 200.
- Lenzen, R., Hartung, M., Brandner, W., et al. 2003, *SPIE Proc.*, 4841, 944
- Macintosh, B., Graham, J. R., Ingraham, P., et al. 2014, *Proc.Nat.Acad.Sci.*, 111, 12661.
- Marino, S., Perez, S., & Casassus, S. 2015, *ApJ (Letters)*, 798, L44
- Milli, J., Mouillet, D., Fusco, T., et al. 2017, *arXiv:1710.05417*
- Milli, J., Engler, N., Schmid, H. M., et al. 2019, *A&A*, 626, A54
- Monnier, J. D., Harries, T. J., Bae, J., et al. 2019, *ApJ*, 872, 122
- Murakawa, K., Suto, H., Tamura, M., et al. 2004, *PASJ*, 56, 509
- Murakawa, K., Suto, H., Oya, S., et al. 2005, *A&A*, 436, 601
- Muto, T., Grady, C. A., Hashimoto, J., et al. 2012, *ApJ (Letters)*, 748, L22
- Norris, B., Schworer, G., Tuthill, P., et al. 2015, *MNRAS*, 447, 2894
- Ohnaka, K., Weigelt, G., & Hofmann, K.-H. 2016, *A&A*, 589, 91.
- Perrin, M. D., Schneider, G., Duchene, G., et al. 2009, *ApJ (Letters)*, 707, L132
- Perrin, M. D., Duchene, G., Millar-Blanchaer, M., et al. 2015, *ApJ*, 799, 182
- Pinilla, P., Benisty, M., de Boer, J., et al. 2018, *ApJ*, 868, 85
- Quanz, S. P., Schmid, H. M., Geissler, K., et al. 2011, *ApJ*, 738, 23
- Quanz, S. P., Avenhaus, H., Buenzli, E., et al. 2013, *ApJ (Letters)*, 766, L2
- Racine, R., Walker, G. A. H., Nadeau, D., et al. 1999, *PASP*, 111, 587
- Safonov, B., Dodin, A., Burlak, M., et al. 2020, *arXiv:2005.05215*
- Schmid, H. M., Joos, F., & Tschan, D. 2006, *A&A*, 452, 657
- Schmid, H. M., Beuzit, J.-L., Feldt, M., et al. 2006, *IAU Colloq.* 200, p. 165.
- Schmid, H. M., Bazzon, A., Roelfsema, R., et al. 2018, *A&A*, 619, 9
- Simmons, J. F. L. & Stewart, B. G. 1985, *A&A*, 142, 100
- Sivaramakrishnan, A., Koresko, C. D., Makidon, R. B., et al. 2001, *ApJ*, 552, 397
- Stolker, T., Dominik, C., Avenhaus, H., et al. 2016, *A&A*, 595, A113
- Suzuki, R., Kudo, T., Hashimoto, J., et al. 2010, *SPIE Proc.*, 7735, 773530
- Tschudi, C., Schmid, H. M. 2021, *A&A* (submitted)
- van Holstein, R. G., Girard, J. H., de Boer, J., et al. 2020, *A&A*, 633, A64
- Wagner, K., Boehle, A., Pathak, P., et al. 2021, *Nat. Comm.*, 12, 922.
- Wiktorowicz, S. J., Millar-Blanchaer, M., Perrin, M. D., et al. 2014, *SPIE Proc.*, 9147, 914783
- Witzel, G., Eckart, A., Buchholz, R. M., et al. 2011, *A&A*, 525, A130